

Detection of stone circles in periglacial regions of Antarctica in UAV datasets

Pedro Pina¹, Francisco Pereira², Jorge S. Marques², and Sandra Heleno¹

¹ CERENA, Instituto Superior Técnico, Portugal

² Institute for Systems and Robotics, Instituto Superior Técnico, Portugal

Abstract. This paper tests three methods, based on template matching, the watershed transform and the sliding band filter, for the identification of stone circles, a natural pattern formed in periglacial regions of the Earth. All the methods take advantage of the 3D shape of the structures conveyed by Digital Elevation Models (DEM). The DEMs were built from millimetric imagery captured by Unmanned Aerial Vehicles (UAV) in Barton Peninsula, King George Island, Antarctica (62°) during a field campaign developed in 2018. The best results were achieved by the sliding band filter method with a F score of 83.9%.

Keywords: Patterned ground · Antarctica · UAV · DEM · template matching · watershed · sliding band filter.

1 Introduction

Stone circles are a type of natural patterned ground formed in periglacial environments easily attracting the attention due to its remarkable circular geometry (Fig. 1). These metric circular shapes, occurring in clusters of tens to thousands of individuals, are formed in frost-susceptible soils due to freezing and thawing cycles [1] in a convection-like circulation of soil in the active layer of permafrost [2]. Besides their evident geomorphic importance, the periodic burial and exhumation of geological materials may play an important role in the soil carbon cycle in connection to permafrost conditions, designating the stone circles as potential paleoclimatic indicators [3]. Although the processes underlying their formation and evolution are relatively well understood [4], their geometric characteristics, dating and seasonal dynamics are supported by sampling and monitoring few circles [5], preventing obtaining robust statistics and an extended spatial analysis of large fields.

Imagery with milli- to centimetre resolution captured by UAV can greatly contribute to a much more complete geomorphic description of this type of patterned ground in large areas giving context to data built at ground-level [6]. The amount of circles involved requires the use of automated methods to make their segmentation, characterisation and also multitemporal monitoring to account for the dynamics of the processes involved. This paper deals only with the initial phase, that is, with the segmentation of the stone circles which, to our knowledge, is addressed for the first time.

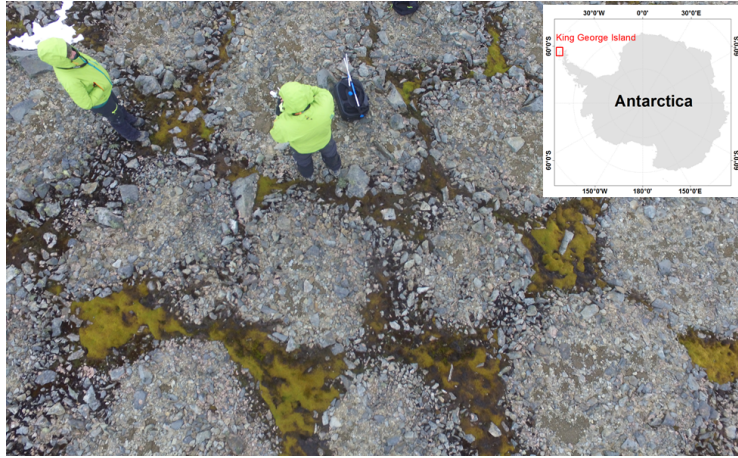


Fig. 1: Stone circles observed from UAV in Barton Peninsula, King George Island (Antarctica), acquired by IST team in February 2018.

2 Data acquisition

The sites selected for developing the surveys are located in Barton Peninsula of King George Island (62°S), Antarctica (Fig. 1). This peninsula is an ice-free area of about 12 km^2 and one of the sites in Antarctica where these natural patterns are more ubiquitous [7]. A field campaign was developed during February 2018 by two of the authors of the current work (PP and SH) with logistics support from the Portuguese Polar Program and the Korean Polar Research Institute. The imagery was acquired with a quadcopter DJI Phantom 3 equipped with a RGB camera at low altitude flights (10 m above ground) to allow perceiving stones up to 5 mm in size. The aerial surveys were planned in a double-grid mode with a high overlap (80%) between adjacent images (lateral and frontal) to provide an increased number of views for the same point. The area surveyed in each individual flight, conditioned by battery duration, is about $80\text{ m} \times 80\text{ m}$ and contains about 500 images. The individual images were processed with *Agisoft Photoscan* software to build orthorectified image mosaics and digital elevation models (DEM) based on SIFT-Scale-Invariant Feature Transform and SfM-Structure from Motion technique. The resolutions obtained are 2.6 mm/pixel for the orthorectified image (typical size of $25,000 \times 25,000$ pixels) and 1.3 cm/pixel for the DEM (5000×5000 pixels). Smaller square regions from the global mosaic and DEM (5000 and 1000 pixels, respectively) were extracted to be processed with circles detection algorithms, as illustrated in Fig. 2.

3 Detection methods

Circular structures can be described by their circular shape patterns although several kinds of deformation can be observed in many images. These deforma-

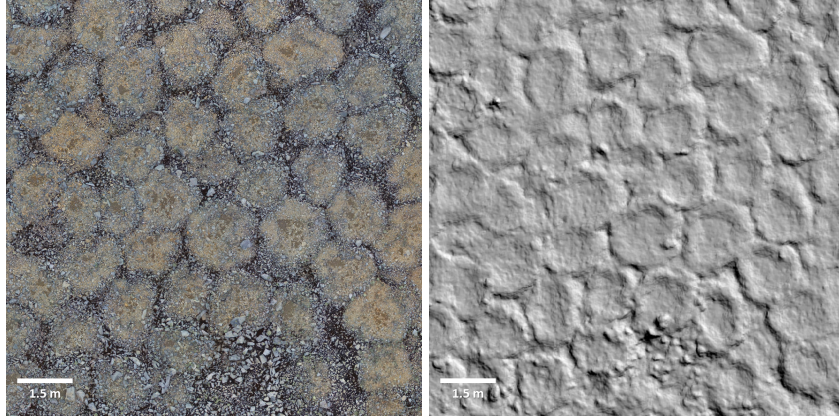


Fig. 2: Detail of orthorectified mosaic (left) and respective DEM (right).

tions are related to the process of structure formation along the years and to the slope of the terrain. In the sequel we will present three detection methods that take into account the 3D shape of the structures to be detected.

3.1 Template matching

Most structures to be detected have a circular shape with a radius that is approximately constant within each site. The radius may change from site to site since it depends on the altitude and characteristics of the soils.

We will assume that the elevation image contain 3D patterns of known shape $T(x, y)$, denoted as template. The fit between the elevation image $I(x, y)$ and the sliding template $T(x, y)$ can be measured by the correlation

$$R(x_0, y_0) = \sum_{(x,y)} I(x, y)T(x - x_0, y - y_0), \quad (1)$$

that achieves a local maximum when the template is aligned with the circle. The template is chosen as a half torus (Fig. 3)

$$T(x, y) = \left(1 - \frac{(r - R)^2}{(\epsilon R)^2}\right)^+, \quad r = \sqrt{x^2 + y^2}, \quad (2)$$

where R is the radius, ϵR is the torus width ($\epsilon = 0.2$), and $x^+ = \max(0, x)$ is the rectifier function.

The detection of circles is based on the analysis of the correlation matrix $R(x, y)$ by detecting all the local maxima (non-maximum suppression), followed by comparison with a threshold T .

Since the elevation image has some natural slope, the image I is first pre-processed by a high-pass filter. The proposed algorithm depends on two parameters (R, T), radius and threshold.

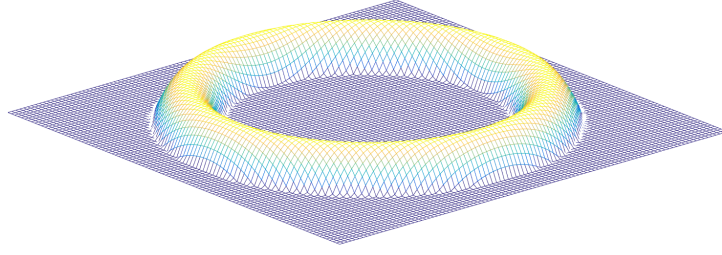


Fig. 3: Template: half torus.

3.2 Watershed

The internal regions of the circles are relatively flat with their edges corresponding to crests in the elevation data. The watershed transform, which simulates the flooding of a surface from its minima, seems adequate to make their segmentation. The watershed (WS) of the elevation image I corresponds to the skeleton of influence zones (SKIZ) of its minima (min) [8]:

$$\text{WS}(I) = \text{SKIZ}(\min(I)). \quad (3)$$

Since not all the minima from the elevation image are interesting, namely the deeper ones normally located outside the circular shapes, its filtering can be performed to leave only (ideally) the shallower ones located within each circle. This procedure is done in two steps. First by increasing the regularity of the circular structures by a morphological filter of the type closing ϕ followed by an opening γ of the elevation image I with a disk B as structuring element

$$I_f = \gamma^B(\phi^B(I)), \quad (4)$$

and then by discarding the minima whose depth or contrast value exceeds the value h . The interesting and shallower minima (\min_S) of I_f are identified through the h-minima transform (HMIN) [8]

$$\min_S(I_f) = \text{HMIN}_h(I_f) = R_{I_f}^{\varepsilon}(I_f + h), \quad (5)$$

where $R_{I_f}^{\varepsilon}(I_f + h)$ indicates the reconstruction by erosion of the marker image ($I_f + h$) into the mask I .

Since it is intended to delineate each circle along its crest line, the minima or seeds upon which the watershed transform will start the flooding procedure are constituted by the union of \min_S and the border lines of their regions of influence, like performed in a similar delineation problem of impact craters [9].

Finally, a post-processing step based on the morphometric features of the detected objects is performed to filter out small and less circular individuals. The size threshold can be easily fixed, but the circularity C obtained by the index that relates the area A and perimeter P of an object ($C = 4\pi A/P^2$) requires some analysis. Therefore this algorithm depends also on two parameters (h, C).

3.3 Sliding band filter

The gradient field of natural circles exhibit radial vector patterns (see Fig. 4). To detect such patterns, we adopt a modified version of the sliding band filter (SBF) proposed in [10] for the detection of cells in microscopy images. The problem addressed in this paper is slightly different, however, since the gradient of cell images points inwards while the gradient of natural circles points inwards and outwards, depending on the distance to the center.

Let us assume that we know the center of the circle $c = [x, y]^T$ and let us define N radial directions starting from c , with angles $\theta_i = 2\pi i/N, i = 0, \dots, N-1$. Along each direction we will measure the alignment between the gradient direction and the radial orientation θ_i , given by

$$A_i(r) = \cos(\phi_i(r) - \theta_i), \quad (6)$$

where $\phi_i(r)$ denotes the direction of the gradient field at a point $c+r[\cos(\theta_i), \sin(\theta_i)]^T$. The gradient orientation changes when the point is located at the circle boundary. To detect the boundary we will perform template matching along each direction and choose the radius r_0 that corresponds to the highest peak. Therefore, the best alignment in direction θ_i is

$$A_i = \max_{r_0} \left\{ \sum_r T(r - r_0) A_i(r) \right\}, \quad (7)$$

where $T = u(r + \Delta) - 2u(r) + u(r - \Delta)$ is the template ($u(r)$ denotes the unit step signal). Since there are N radial directions, the global alignment is the sum of all the directional alignments

$$A = \sum_{i=0}^{N-1} A_i. \quad (8)$$

The previous expressions provide the alignment score associated to the center hypothesis $c = [x, y]^T$. In practice we do not know c . What we do is to compute

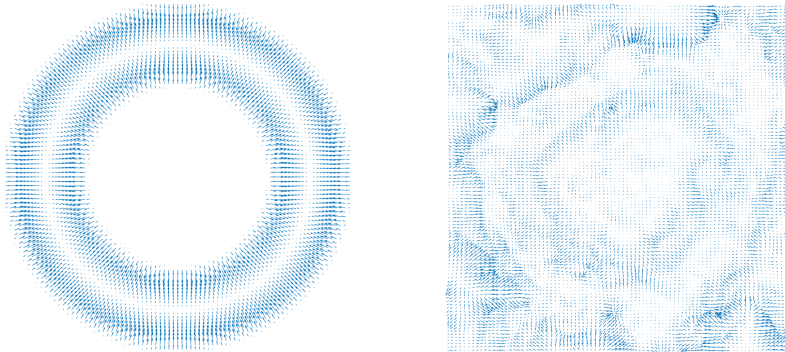


Fig. 4: Gradient field of torus (left) and natural stone circle (right).

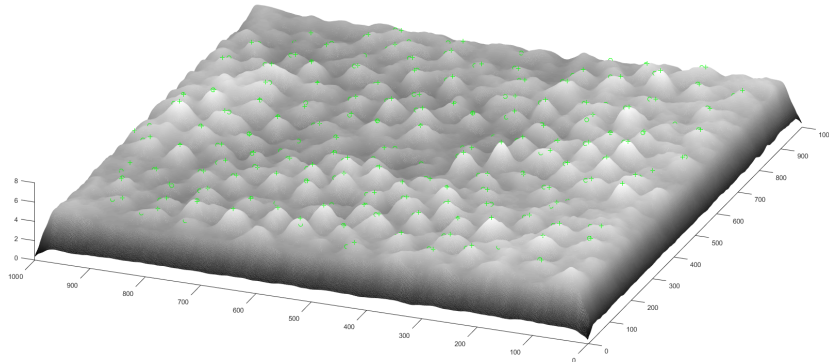


Fig. 5: Alignment score as a function of the circle center.

the alignment score for each image point, c , and detect the circle centers by non-maximum suppression and thresholding (see Fig. 5).

To be specific, the gradient vector is computed by using Sobel masks and its magnitude is compared with a threshold: gradients with small magnitude are discarded.

4 Results

The algorithms were evaluated on a dataset of six DEMs from two sites, with size 1000×1000 pixels. These images include a variety of cases ranging from regions with a stationary quasi-periodic structure to highly unorganized regions.

4.1 Performance measure

To evaluate the performance of the proposed algorithms, ground truth (GT) information was built by visually detecting all the circles and annotating their centers.

Since the algorithms also produce a set of centers, we need to establish a correspondence between the detected centers and the ground truth information. This was achieved by using a simple matching algorithm defined as follows. First, we build a matrix of distances from all the GT centers to all the detected centers. The minimum element of the matrix is found (excluding the diagonal elements) and the corresponding points are matched, provided that the minimum distance is smaller than a threshold Δ . If two points are matched they are considered as a true positive (TP) detection and the corresponding line and column are removed from the distance matrix. The process is repeated until there are no more candidates for matching. The ground truth points which were not matched are considered as false negatives (FN) and the detected points that were not matched are considered as false positives (FP).

Table 1: Performance measures of template matching, watershed and sliding band filter (SBF) methods: mean and standard deviation computed in six images.

Methods	Precision (%)	Recall (%)	F (%)
Template matching	69.6 (10.5)	73.8 (14.1)	70.3 (8.1)
Watershed	65.2 (12.3)	79.5 (7.0)	71.3 (9.7)
SBF	78.5 (6.3)	90.5 (6.0)	83.9 (4.5)

The performance of the detection algorithm is characterized by the well known measures

$$\text{Precision} = \frac{TP}{TP + FP}, \quad \text{Recall} = \frac{TP}{TP + FN}, \quad (9)$$

$$F = 2 \frac{\text{Precision} \cdot \text{Recall}}{\text{Precision} + \text{Recall}}. \quad (10)$$

The F-score combines the precision and recall in a single measure.

Fig. 6 shows the performance of the proposed methods in two images extracted from different sites. The example on the left is well organized and quasi-periodic while the example on the right is much more difficult. For each example we show the ground truth information (circles), the detected objects (crosses) and the TP (green), FN (yellow) and FP (red). In the case of the watershed and SBF methods, we also show the circle boundaries (yellow). All the methods detect most of the natural circles present in the image, despite the fact that the dynamic range presents small changes on the order of centimetres.

4.2 Statistical evaluation

The parameters associated with each method were chosen experimentally: $R = 35$ pixels, $T = 0.4$ for template matching method, $h = 10$ cm, $C = 0.70$ for watershed method, and $N = 16$, $\Delta = 7$, threshold= 70% of maximum peak amplitude for SBF method. Then, we processed the six images with the three methods and for each image we computed precision, recall and F-score. The mean and standard deviation of all these measures are shown in Table 1. The best results were obtained by SBF method which achieves a F-score = 83.9%. The template matching and watershed method achieve worse performances (F-scores = 70.3% and 71.3%, respectively).

Fig. 7 displays the three statistics (precision, recall and F-score) obtained by the three methods in each of the test images highlighting the superiority of SBF method.

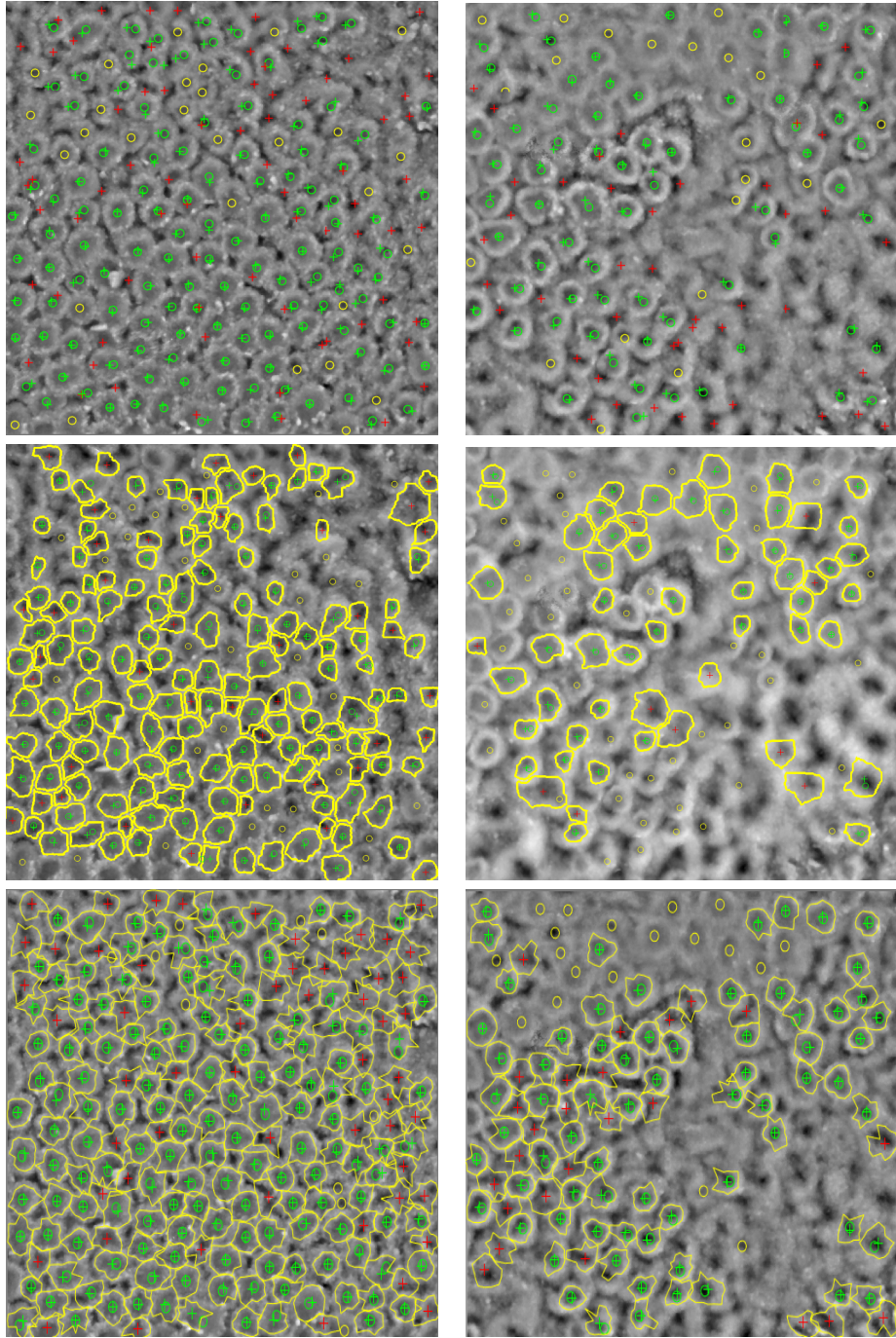


Fig. 6: Examples from 2 field sites: outputs of template matching (top), watershed (middle) and SBF (bottom). Colour code: true positives (green), false positives (red) and false negatives (yellow).

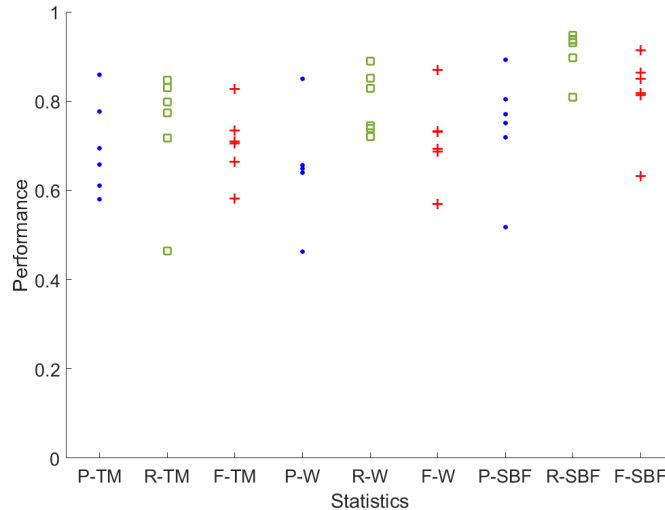


Fig. 7: Precision (blue point), recall (green square) and F score (red cross) for the three methods in each of the six images.

5 Conclusions

This paper presents a new problem: the detection of stone circles in periglacial terrains. The information used to estimate such structures consists of elevation data built after optical imagery, captured by a UAV in Antarctica (Project CIRCLAR2 from the Portuguese Polar Program).

The structures have a circular shape, exhibiting several types of deformation due to the natural processes involved in their formation and development along centuries. Three automatic algorithms are described, exploiting the shape information, based on template matching, watershed transform and sliding band filter (SBF). The methods are evaluated in six elevation images (1000×1000 pixels) achieving an F score ranging from 70.3% to 83.9%. The best results were achieved by SBF method that clearly outperforms the other two. This is probably related to the assumptions made in each method. Template match makes strong rigidity assumptions about the object shape, the watershed-based is probably too flexible. The SBF filter presents a more appropriate trade-off between shape assumptions and deformation.

There are several open issues to be addressed in the future. One concerns shape deformation. The assumption of rigid scales adopted in template matching is perhaps too hard and should be studied. A second issue concerns multiple scales since the size of the natural circles change, depending on the type of material and altitude. One promising direction for future research concerns the combination of multiple detection algorithms and the use of multi-scale methods.

Acknowledgements. This work was supported by FCT plurianual funding (UID/EEA/50009/2019 and UID/ECI/04028/2019), project CIRCLAR2 (call 2017-2018 from PROPOLAR-Portuguese Polar Program) and KOPRI-Korean Polar Research Institute for logistics at King Sejong Station in Antarctica, and FCT project SPARSIS PTDC/EEIPRO/0426/2014.

References

1. Washburn A.L. (1980) *Geocryology: a survey of periglacial processes and environments*. New York, Wiley.
2. Hallet B. (2013) Stone circles: form and soil kinematics. *Philosophical Transactions of the Royal Society A*, 371, 20120357.
3. Kaab A., Girod L., Berthling I. (2014) Surface kinematics of periglacial sorted circles using structure-from-motion technology. *Cryosphere*, 8, 1041-1056.
4. Kessler M.A., Murray A.B., Werner B.T., Hallet B. (2001) A model for sorted circles as self-organized patterns. *Journal of Geophysical Research - Solid Earth*, 106, 13287–13306.
5. Jeong G.Y. (2006) Radiocarbon ages of sorted circles on King George Island, South Shetland Islands, West Antarctica. *Antarctic Science*, 18, 265–270.
6. Pina P., Vieira G., Bandeira L., Mora C. (2016) Accurate determination of surface reference data in digital photographs in ice-free surfaces of Maritime Antarctica. *Science of the Total Environment*, 573, 290-302.
7. López-Martínez J., Serrano E., Schmid T., Mink S., Linés C. (2012) Periglacial processes and landforms in the South Shetland Islands (northern Antarctic Peninsula region). *Geomorphology* 155–156, 62–79.
8. Soille P. (2003) *Morphological image analysis. Principles and applications*. 2nd edition, Berlin-Heidelberg, Springer.
9. Pina P., Marques J.S. (2013) Delineation of impact craters by a mathematical morphology based approach. In M. Kamel and A. Campilho (Eds.): ICIAR2013, LNCS 7950, 717–725.
10. Quelhas P., Marcuzzo M., Mendonça A. M., Campilho A. (2010) Cell nuclei and cytoplasm joint segmentation using the sliding band filter. *IEEE Transactions on Medical Imaging* 29(8), 1463-1473.